NIOBIUM COMPOUNDS IN ACOUSTICS AND ELECTRO-OPTICS

Dieter H. Jundt

Crystal Technology, Inc.
1040 E. Meadow Circle
Palo Alto, California 94303, U.S.A.

Abstract

Niobium containing oxide crystals generally are ferroelectrics with useful applications in acoustics, nonlinear optics and electro-optics. Crystal growth technology for lithium niobate has reached a state where 125mm diameter wafers are easily available. This material is used mostly in surface acoustic wave filters for TV IF filters. Much growth in demand for lithium niobate wafers is seen from the manufacturing of high speed digital modulators for telecommunication systems. Other uses such as birefringent prisms, bulk acoustic transducers are also discussed. The other niobates typically crystallize in the perovskite structure, and growth is much more challenging because of structural phase-transitions and the absence of a congruent composition. Some of the crystals studied include potassium niobate (KN) or KLN for blue light generation, SBN or KN for photorefractive applications, and relaxor ferroelectric crystals for highly efficient actuators and ultrasonic transducers.

Introduction

Niobium oxide containing crystals exhibit interesting behavior due to the strong hyperpolarizability of the Nb-O bonds. The bond polarizes more easily, i.e. the electronic charge shifts more easily, when the electric field is applied in a specific direction. In a centro-symmetric crystal configuration, the asymmetry of one bond is canceled out by that of a corresponding bond pointing in the opposite direction. Only in crystal structures that lack inversion symmetry do the polarizabilities add up to yield macroscopically observable effects. The most studied niobium oxides all belong to the class of ferroelectrics. In the high temperature (para-electric) phase, the crystal has inversion symmetry, but as the crystal is cooled below the Curie temperature, it undergoes a phase transition to the ferro-electric phase. This transition is caused by a displacement of the cations with respect to the oxygen lattice as shown in Figure 1 for the case of lithium niobate (1).

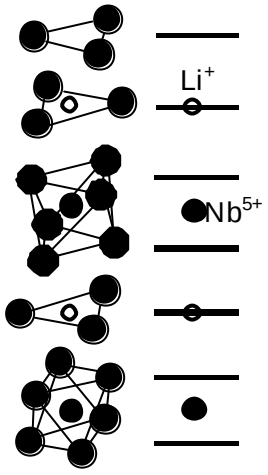

Figure 1a: Schematic representation of the para-electric phase of lithium niobate. The oxygen planes are represented by lines, with the cations centered on, or between the planes.

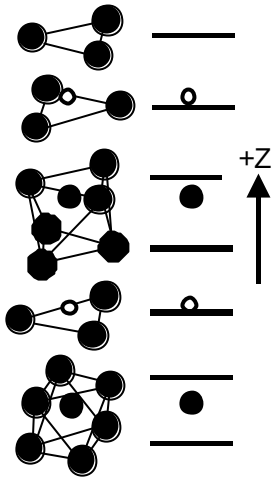

Figure 1b: Schematic representation of the ferro-electric phase ($T<T_c$=1142°C). The cations are displaced from the center position, defining the direction of the polar Z-axis.

Within a domain, all the cations are displaced in unison in one direction, giving rise to a spontaneous polarization (at no applied field) in that direction. Neighboring domains have displacements pointing in a different direction. As-grown crystals typically show a multi-domain behavior, precluding any useful applications. The domains can be decorated by etching a polished surface due to a differential etch rate for opposing polar faces. Such an etch pattern is shown in Figure 2 (2).

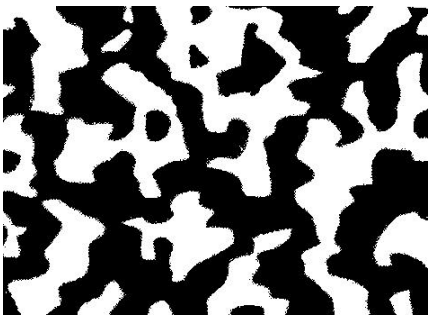

Figure 2: Domain pattern on unpoled lithium niobate. Dark areas are –Z faces that etch rapidly and thus appear rough and do not reflect as much light. The field of view covers about 400 microns.

Perovskite ferroelectrics such as $KNbO_3$ (KN) or $BaTiO_3$ undergo several different phase transitions as they are cooled (3). The high temperature phase is cubic with the Nb atom centered in the lattice. At the Curie transition, it displaces along one of the sides of the cube, resulting in a tetragonal structure. Any of the 6 faces of the cube are possible directions for the spontaneous polarization. As the crystal is cooled further, the direction of displacement changes, now pointing towards the center of one of the edges of the cube, a phase-transition to a orthorhombic structure. This structure has 12 possible directions for the spontaneous polarization. A further phase transition to a rhombohedral structure occurs as the spontaneous polarization orients itself toward the corners of the cube. Those transitions involve length changes in the crystal lattice along and perpendicular to the spontaneous polarization. The tetragonal lattice for example is stretched along the polar axis, and slightly contracts in the other two dimensions. As neighboring domains are created with different direction of spontaneous polarization, stress is induced that often leads to fracturing of the crystal. The sequence of phases with the transition temperatures is shown in
Figure 3 for the case of $KNbO_3$. A KN crystal at room temperature has undergone two phase-transitions.

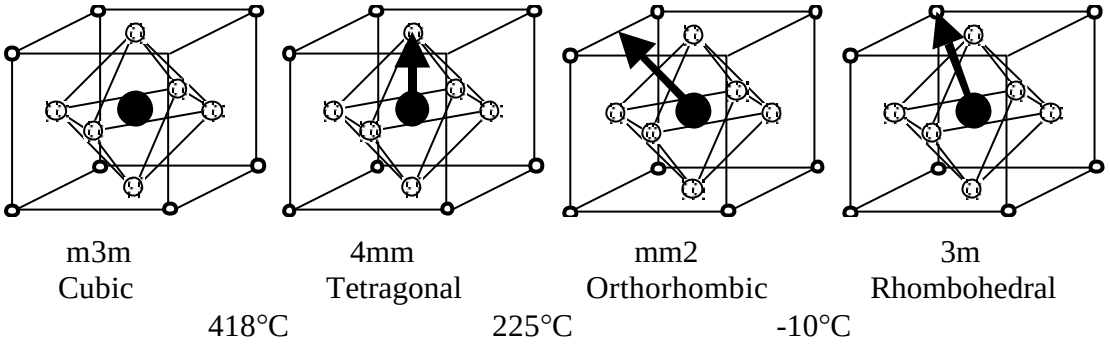

Figure 3: Sequence of symmetry changes as $KNbO_3$ is cooled. The black arrow denotes the direction of the spontaneous polarization (displacement of Nb).

The ferroelectric crystals $LiNbO_3$ and $LiTaO_3$ have a trigonal (three-fold rotation) symmetry in the high temperature phase as shown in Figure 1. On cooling, the spontaneous polarization aligns with this symmetry axis, so only two directions are possible. Consequently, no further phase transition is observed below the Curie temperature, and there is no structural mismatch between neighboring domains. This allows the production of large crystals without the risk of fracturing at the phase transition temperature. This has enabled commercial development with applications in mass-market appliances such as TVs and mobile phones.
To be useful, uniformly poled crystals are desired where the whole crystal has a spontaneous polarization pointing in the same direction. This can be achieved by a poling step after growth. An electric field is applied while the crystal is cooled through the phase transition temperature (Curie temperature). At that temperature, the developing spontaneous polarization will align itself along the polarization induced by the applied field, and a single-domain crystal results.

The polar nature of a crystal in a ferroelectric phase gives rise to third-order tensor material properties, such as piezo-electric, electro-optic and nonlinear optic effects. Second order tensors are also affected with the properties along the polar axis being different from those for other directions (4). Many of these effects are enhanced in proximity to phase transition temperature. Mixed crystals such as $K_xLi_{1-x}NbO_3$ or $Sr_xBa_{1-x}NbO_3$ have adjustable Curie temperatures and show large effects at room temperature.

Lithium Niobate and its Applications

Devices manufactured of lithium niobate (LN) are used in many products such as surface acoustic wafer (SAW) filters, integrated optic devices, birefringent elements in optical read heads, and blur-filters for digital cameras. Applications using smaller volumes of LN include nonlinear- and electro-optic devices, and transducers for acousto-optic cells. As of this writing, over 80 tons of LN per year are grown and fabricated into wafers worldwide. Those applications relie on the useful macroscopic properties: A large birefringence (~0.1) enables production of small polarizing elements, the piezo- and electro-optic effects enable the production of SAW filters and integrated optics devices. As shown in Figure 4, two other factors also influence the material's commercial viability: Growth of large and uniform crystals is possible yielding crystals with reproducible material properties, allowing efficiency of scale. The material is easily processed and polished, enabling simple manufacturing methods to produce devices. Other ferroelectric materials such as those mentioned below might have better figures of merit for particular applications, but often are not easily grown or have phase transitions within customarily utilized processing temperatures.

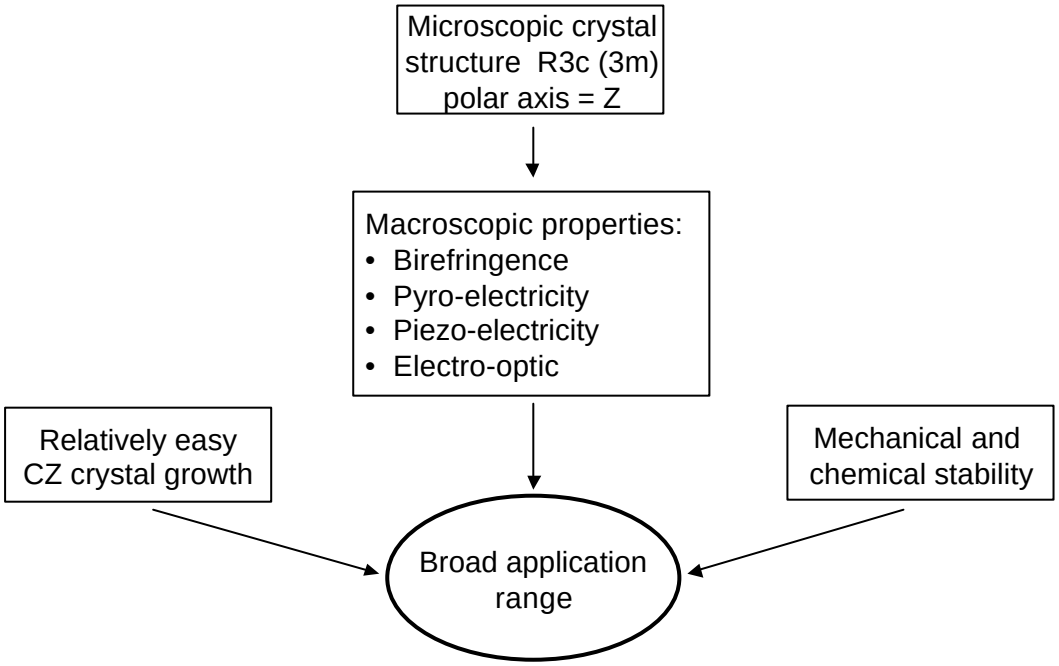

Figure 4: Combination of factors that have enabled LN to be the most widely used ferroelectric crystal.

Growth of Lithium Niobate Crystal

LN is grown using the Czochralski method, widely used for industrial crystal growth, most notable that of Silicon (Figure 5). The pure compound of the material to be grown is melted in a crucible in the growth station. A seed crystal suspended from a rotating seed rod is then lowered into the furnace cavity, and the tip is touched into the melt. If the melt temperature is in the appropriate range just slightly above the melting point of the compound (1250°C for LN), growth of a crystal can be initiated by starting to slowly withdraw the seed rod. New crystal material will attach to the solid seed that is cooled by conducting heat through the seed rod. As the growth progresses, the diameter of the growing crystal is controlled by adjusting the heating to the crucible. Lowering the heat input will accelerate the crystallization and lead to a diameter increase, while increased heat will act to decrease the crystal diameter. Growth

furnace configurations and parameters for successful LN growth have been described by various groups (2, 5-7).

Figure 5 shows a schematic of a furnace with induction heating. The thermal environment together with growth parameters such as rotation rate and crystallization speed determine the crystal quality. High radial gradients generally lead to high strain, often resulting in crystal cracking on cool-down (8, 9).

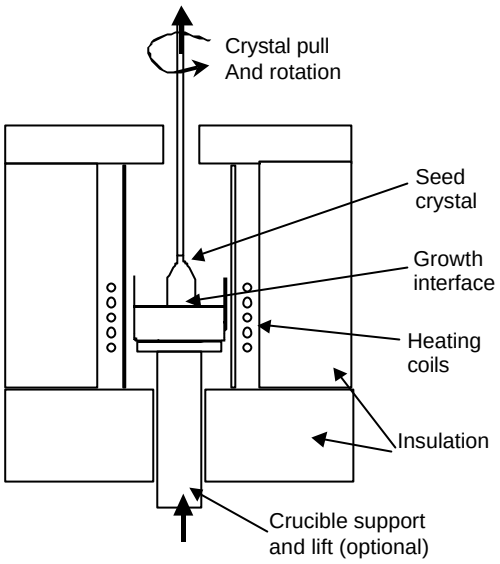

Figure 5: Schematic cross-section of a Czochralski growth furnace. The crystal is pulled from the melt.

The starting melt typically is prepared by loading the crucible with pre-reacted LN powder, and melting it in consecutive heating runs so that the crucible can be filled to the desired level. The starting materials for the reaction are lithium carbonate and niobium pentoxide. The purity of the starting materials needs to be very high (4-9s or better) for optical quality crystals, or if a large fraction of the melt is to be converted into the crystal. Transition metal impurities lead to optical absorption in the visible and near infrared range of the spectrum, and impurities such as Ca will be rejected by the growing crystal with the resulting impurity accumulation in the melt causing veiling at the bottom of the crystal. As shown in Figure 6, LN exists over a wide range of compositions. Only a crystal grown at the congruency composition will be uniform along the growth axis. At the congruent point, the solid crystal and the liquid have the same composition and are in thermodynamic equilibrium. This allows crystallization of material at the same composition as the melt, and a crystal of uniform composition is pulled. If the melt deviates from congruency (e.g. for stoichiometric composition of $x=c_{Li}/(c_{Li}+ c_{Nb})=50\%$), the starting composition grown also deviates from congruency, but to a smaller degree. For a lithium-rich melt, the excess lithium oxide in the melt is rejected by the crystal and accumulates in the melt at ever increasing amounts as the growth progresses. The resulting crystal will have a compositional gradient along the growth direction. The closer the starting composition comes to true congruency, the faster the growth can proceed and the bigger crystals can be grown without adverse effects such as cracking or inclusions. Accurate weighing of the starting compounds generally includes control of adsorbed water and isotopic ratio determination of Li in Li_2O (2, 10). Deviations from congruency will result in wafer to wafer variations in important material properties such as sound velocity, Curie temperature, birefringence etc.(10-13).

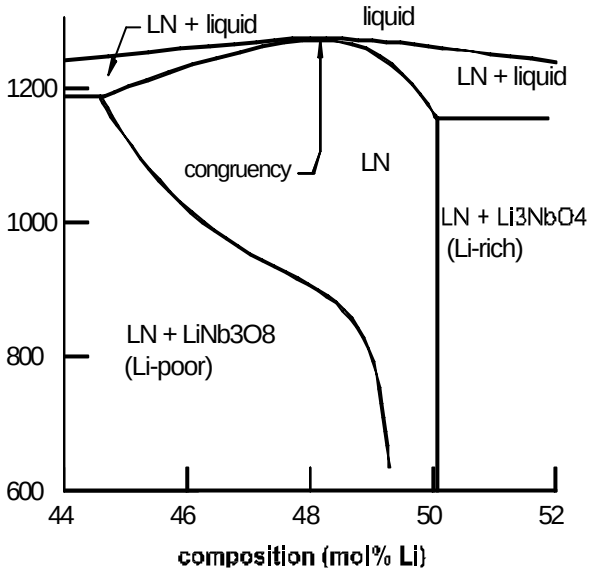

Figure 6: Phase diagram of LN. Growth ideally takes place at the congruency point.

Wafer Fabrication

Most LN today is consumed in the form of wafers with at least one surface polished. Wafers are ideally suited for mass fabrication processes involving lithography with subsequent coating steps. These technologies have been pioneered and refined for VLSI manufacturing on silicon. As the device scale continues to get smaller, the requirements for surface quality, cleanliness, and wafer flatness become more demanding. As the price per chip needs to decrease, the wafer size must increase so that more chips can be processed together in the same processing steps. LN is undergoing the same evolution as silicon, albeit somewhat delayed in time. The most commonly used wafer diameter in LN today is 100mm, with some customers transitioning to 125mm (silicon currently is transitioning to 300mm).

For high volume wafer manufacturing, the material utilization needs to be optimized and the process automated as much as possible. The wafer thickness varies depending on the application. Thicker wafers (typically 1mm) are more costly, but are more rigid with a smaller chance of handling-induced breakage. The most commonly used thicknesses for SAW wafers are 0.35 and 0.5mm. Most lithographic applications do not require the back surface to be polished, so that only one side needs to be polished, with the back surface typically in an as-lapped state. The crystals of cylindrical shape are grown in the orientation most suitable for efficient wafer manufacturing. For example, in the case of the 128° RY wafer orientation, the wafer normal and the cylinder axis are perpendicular to the crystallographic (10.4) plane. After growth and poling, the crystals are ground into a perfect cylindrical shape with a diameter slightly larger than the finished wafer diameter. This is done on fixed diamond abrasive wheels using aqueous coolant. Orientation flats are then ground along the cylinder sides with similar equipment.

There are two technologies used for wafer slicing: annular saws and wire saws. In an annular saw, the saw blade is held and tension applied around its outside perimeter. This gives the thin blade the required stiffness. The inner rim of the central hole in the saw blade is coated with electro-phoretically deposited diamond. Using this saw, each wafer is cut individually. Wire slicing was developed for large diameter silicon wafers that can not be cut on annular saws. In this process, a continuous wire is wound around several grooved guide-rolls. The resulting "web" between two of those guide-rolls can be up to 400mm long consisting of hundreds of

wire segments. As the steel wire is stretched with high tension and transported at speeds up to 15m/s, cutting is performed by loose abrasive (SiC) delivered in a suspended slurry of either glycol or oil (14). Wire slicing has the advantage of smaller kerf loss, can be scaled to larger wafer sizes, and has the potential for lower warp and better surface finish of the sliced wafers. Several hundreds of wafers can be sliced in a single run taking a few hours. After slicing, the perimeter is re-machined to avoid having edge cracks propagate in subsequent processing steps. This operation is done by hand (beveling), or by automated edge-grinding machines, having a grinding wheel with embedded diamond and grooves of the desired contour.

The sliced surface is not well suited to be polished directly. A lapping step is used to ensure reproducible roughness and good thickness control. The finer the abrasive used for the lapping step, the less material has to be removed in the time-intensive polishing process. Lapping can be performed in multiple steps with decreasing abrasive size. Most common in production are double-sided lapping machines, using a loose abrasive slurry. The wafers are held inside carriers, which are rotated by the sun and ring gears as the upper and lower plates rotate separately from the carriers. Batches of tens to hundreds of wafers (depending on the machine and wafer sizes) are typically processed simultaneously in one run of 10-15 minutes. Single-side polishing machines mount the wafers onto flat plates which are then rotated against the polishing pad. Wafers are either wax mounted or positioned by templates and held in place by capillary action between the wafer and the template backing. Double-side polishing machines are similar in design, size and capacity to double-side lapping machines, and can achieve better parallelism than the single-side polishing machines. The choice of mounting and polishing supplies as well as the polishing parameters such as pressure and rotation rates influence the removal rate, surface quality and flatness of the wafers. Traditionally, scrubbers have been used for the final cleaning step; however, the increasing demands for better cleanliness, coupled with recent advances in sonic cleaning technology, favor the implementation of ultrasonic and megasonic systems.

Crystal Properties and Application Areas

Birefringent Elements. LN has a large index of refraction (2.2) and high birefringence, i.e. difference in refractive index for light polarized along the polar axis (n_e) from that polarized in the X-Y plane (n_o) (15). For a crystal plate where the surfaces form a 45° angle to the polar axis, randomly polarized light is separated into two beams propagating a slightly different angles through the plate. The two exiting light beams are individually polarized, and also displaced from each other. The figure of merit (displacement for a given thickness plate) roughly scales as $(n_e-n_o)/(n_e+n_o)$. LN has a figure of merit roughly 6 times that of quartz, but smaller than that of Yttrium vanadate. Such walk-off plates are used in high-end digital still-cameras. Aliasing is an undesired effect in digital pictures: A pattern in the scene being photographed with a spatial period too fine to be resolved by the CCD pixels will lead to lower-period artifacts unless the scene is filtered by a spatial low-pass filter (16). The filters consisting of several thin walk-off plates are placed in front of the CCD array. Three correctly oriented plates will "smear" out each ray of light in a hexagonal pattern. Another use for birefringent elements made of LN is in fiberoptic polarizers such as that shown schematically in Figure 7. The light from the telecommunication fiber is randomly polarized. The first prism separates the two polarization states, and displaces them from each other. The two beams also exit the prism at slightly different angles. The Faraday rotator then turns the polarization state of each beam by 45°, and the second LN prism, oriented with axes aligned to this light, recombines the two polarization states into the fiber. Light traveling from the other direction will incur the same effects, but instead of the second prism compensating for the first one, it adds to the angle so that the light completely misses the fiber.

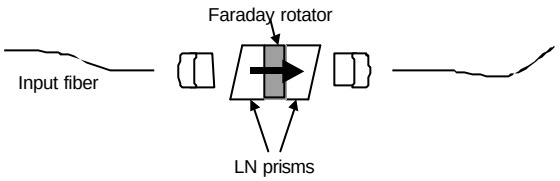

Figure 7: Schematic of fiber-optic isolator.

Nonlinear Optics. One of the first suggested uses for LN was in nonlinear optical interactions (17, 18). Because of the nonlinear character of the polarizability, a strong optical field at frequency ω produces a polarization at frequency 2ω. If this polarization is produced with the correct phase at every given location in the crystal, a strong optical beam is generated and a significant amount of energy is produced at the second harmonic frequency. This phase-matching only can take place if the interacting waves are propagating at the same speed, i.e. if the refractive index of the incident beam and the generated second harmonic beam see the same index of refraction. Because of dispersion, this is not the case in a typical material. One possibility to achieve phase-matching is to utilize the birefringence of the crystal to offset dispersion.This is shown in figure 8 for 5% MgO doped LN at room temperature. To phase-match a slightly different wavelength (e.g. 1.064μm emitted from a Nd:YAG laser), the temperature can be adjusted, a process called temperature tuning (18-20).

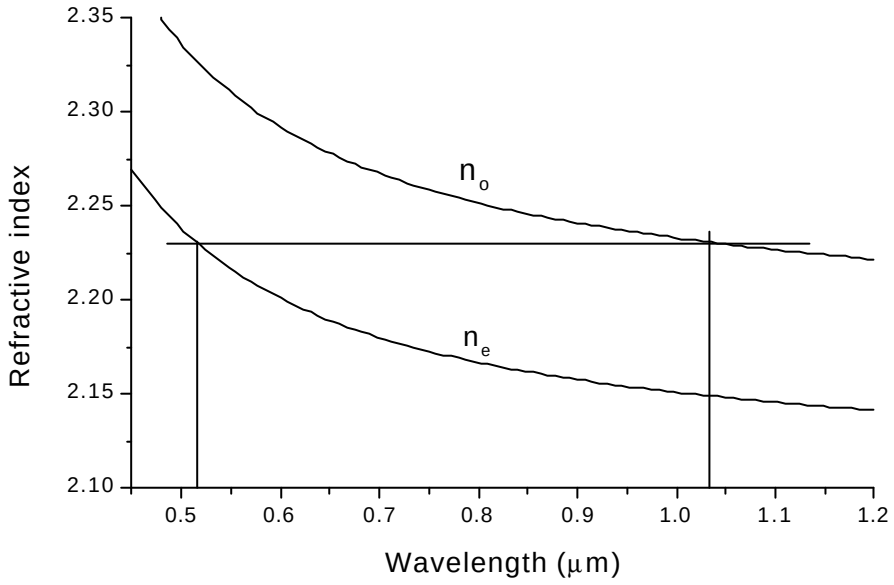

Figure 8: Refractive index curves for ordinary and extraordinary index in MgO:LN. Phase-matching is satisfied for λ=1.029μm where $n_o(\lambda) = n_e(\lambda/2)$.

LN is not widely used in nonlinear optics. Undoped crystals display strong photorefractive behavior in the presence of green or blue light, distorting the laser beam grossly (21, 22). Magnesium doping raises the threshold for this effect considerably, and frequency-doubling in that material has found some applications.

Birefringent phase-matching as described above has only a very limited range of wavelengths that can be covered. Periodic poling of LN (PPLN) allows quasi-phase-matching extending the range of wavelengths tremendously. To produce periodically poled crystals, a uniformly poled LN crystal is first patterned with electrodes of the desired periodicity. An electric field exceeding the coercive field is then applied, and the spontaneous polarization under the

electrodes reverses (23). In a typical application, all interacting waves are polarized along the polar axis. Because of dispersion, the waves are not phase-matched. However, by choosing the correct period for poling, the waves can still interact efficiently (24). PPLN crystals have been used for optical parametric oscillators generating tunable radiation in the mid infrared region of the spectrum. Such sources have applications in counter-measures for simple heat-seeking missiles and in spectroscopy (25, 26).

Holographic data storage. The photorefractive effect mentioned above can be utilized to store information in a crystal. Iron impurities act as electron donors when illuminated with green or blue light (27). These electrons drift until they are trapped by a point defect such as a Nb_{Li} antisite defect. The trapping is more likely to occur in dark regions of the crystal, building up space-charge fields that are related to the light intensity pattern. This sequence of events can be interpreted as the "writing" of a hologram. The charge fields modulate the refractive index via the electro-optic effect, and can be "read out" by a probe beam, retrieving the information stored. Many experiments have been described over time utilizing this effect. One of the challenges is that the reading process often erases the hologram. Also, dark conductivity and thermal excitation of the trapped electrons will eventually erase the hologram. A solution to this problem is a process called "fixing" of the hologram:(28) The crystal is heated up so that the proton impurities or Li^+ ions move to compensate the stored electronic space charge (29). After this baking step, the crystal is uniformly illuminated to re-distribute the electronic charges, leaving the ionic hologram behind that is resistant to erasure by illumination (30). Storage lifetimes depend strongly on defect concentrations that are difficult to control,(28) and LN consequently has not been commercially utilized in such storage systems. Another hurdle for commercialization of holographic systems based on LN is the need for an expensive green and powerful laser to write the holograms. Applications that write and fix the hologram in the factory, and only read out information in the actual application have a better chance of commercial success. One such scheme involves recording permanent gratings to selectively reflect certain wavelengths of a wavelength division multiplexed fiber-optic communication system (31).

Acousto-optics. Bulk acoustic waves can be excited in a piezo-electric crystal by applying an electric field across the thickness of the thin plate. LN supports longitudinal as well as two types of shear modes. A free plate will have a resonance frequency $\nu=c/2d$ where c is the speed of sound and d the thickness. A schematic of an acousto-optic device is shown in Figure 9 (32). The most commonly used transducer material is a 36° rotated Y plate of LN, metallized on both sides. The transducer is excited in a thickness excitation mode, and the electromechanical coupling factor is 49% for this orientation. The transducer thickness is chosen to match the frequency needed for the acoustic wave. Efficient diffraction requires the Bragg condition to be satisfied. To avoid standing wave patterns, the far end of the acousto-optic medium is angled. Acoustic absorbing materials may also be applied to that face of the cell. Acousto-optic cells are used inside laser cavities as Q-switches, or externally as modulators and deflectors. Modulators and deflectors today are mostly used by the digital printing and semiconductor inspection industries. The diffraction efficiency is determined by the design, the acousto-optic material, and the strength of the acoustic wave (33). The acousto-optic material is chosen so as to give a large refractive index change for a given acoustic energy. TeO_2 is a common choice allowing large diffraction angles and good efficiencies at moderate power levels. Crystalline or fused quartz is often used for short wavelength applications.

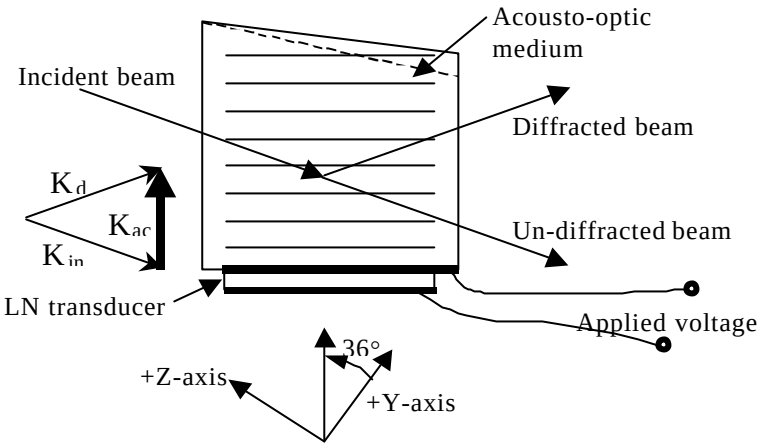

Figure 9: Schematic of acousto-optic cell. Bragg condition is achieved for $k_d = k_{in} + K_{ac}$, enabling efficient diffraction. Among other factors, the strength of the acoustic wave determines the diffraction efficiency.

Surface Acoustic Waves. SAW devices account for the large majority of processed LN wafers worldwide. Most of the wafers go into consumer electronic applications as band-pass filters. Each TV or VCR has intermediate frequency (IF) filters aiding in channel selection. Mobile phones often have front end filters in addition to IF filters (34, 35). Other applications such as delay lines, oscillators or sensors are also possible, but are more often produced on quartz substrates rather than LN.

Surface waves, also called Rayleigh waves, were first described by Lord Rayleigh in 1885. These waves propagate along a half-space, with the particle motion in the plane containing the surface normal and propagation direction. The amplitude of motion is largest at the surface, and decreases exponentially with increasing depth. The most damaging earthquake waves are Rayleigh waves. SAW waves on piezoelectric substrates became important with Radar developments, an area extensively studied through the 1960's (36).

Figure 10 shows a schematic of a simple SAW band-pass filter. The interdigital transducers convert electrical signals to SAW waves efficiently for a SAW wavelength equal to distance between the centers of neighboring electrodes. The transducer on the left will generate SAW waves of equal strength propagating to the left and right. Since the wave traveling towards the edge must be absorbed, this process involves an automatic loss of 3dB, even for perfect conversion from electrical to acoustic wave energy at the peak of the pass band. The identical transducer on the right also incurs a 3dB attenuation when converting the wave back to the electrical output signal, adding 6dB to the electrical insertion loss. The frequency response of the filter can be analyzed approximately by taking advantage of the fact that it is related to the Fourier transform of the transducer pattern (37). In the example given in Figure 16 the transducer area is a rectangle, and the frequency response drops off as $\sin(\nu)/\nu$ from its peak. To produce a better filter with a flat response within the passband, sharp edges and good rejection out of the passband, the transducer strength needs to changes as $\sin(x)/x$. This can be achieved by varying the overlap of the transducer fingers as shown in Figure 11, a technique known as apodizing. Also shown in Figure 11 is an example of a single-phase unidirectional transducer (SPUD). The transducer has built-in reflectors that cancel out the excitation for acoustic propagation in one of the two directions (38). In the example shown, a second metallization step alters the coupling parameters for half the fingers. Other designs for SPUDs are possible, but all require finer finger linewidths than a bidirectional transducer.

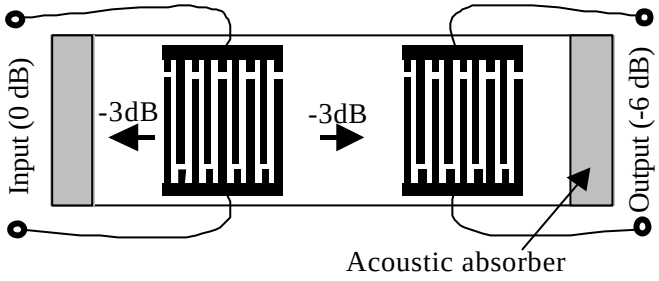

Figure 10: Schematic of simple SAW bandpass filter. Both transducers incur a 3dB loss because they are emitting and receiving the SAWs to both sides.

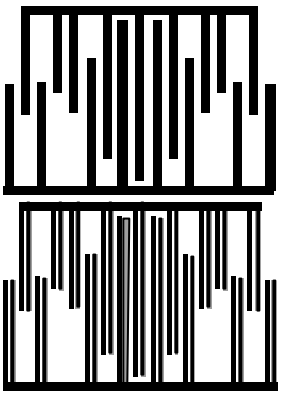

Figure 11: Apodized electrode pattern for interdigital transducer. The strength of excitation varies with the overlap, approximating a sin(x)/x function to give a flat frequency response. Example of SPUDT design where half the interdigital fingers are double-metallized. Such a design allows the acoustic wave energy to be radiated to one side only.

Design of SAW devices is very dependent on good numerical models. The Fourier analogy mentioned above is inadequate for today's designs because of several higher order effects: Each electrode finger interacts with the propagating waves, partially reflecting them, and converting some of the energy back to electrical signals. The limited length of the overlapping transducers gives rise to diffraction. SAW propagation is not a simple one-dimensional problem. Reflected bulk waves (e.g. from the back surface) can also influence the filter performance.

To manufacture SAW filters, the wafers are typically metallized first. The lithography step can use a contact mask-aligner, bringing the wafer in contact with the mask, or a projection system that exposes the pattern either onto the whole wafer, or in a step and repeat operation exposing individual segments of the wafer at a time. After developing the resist, the metal is etched off in the unprotected areas. Other processes such as second metallization steps or deposition of acoustic absorber material follow. After wafer scale testing, the wafers are diced into individual dies that are packaged and wire-bonded. An alternative to wire bonding is the flip-chip technique where solder bumps are defined on the wafer that then are directly mounted onto the package. SAW designs are continuously improved so that the filters become smaller (important for mobile communication devices) and have improved filter characteristics at lower insertion loss. The spectral response of a modern SAW filter is shown in Figure 12. The frequency response is flat over a 34 MHz range with variation of less than 1dB in the passband. This device is made from Y-Z LN.

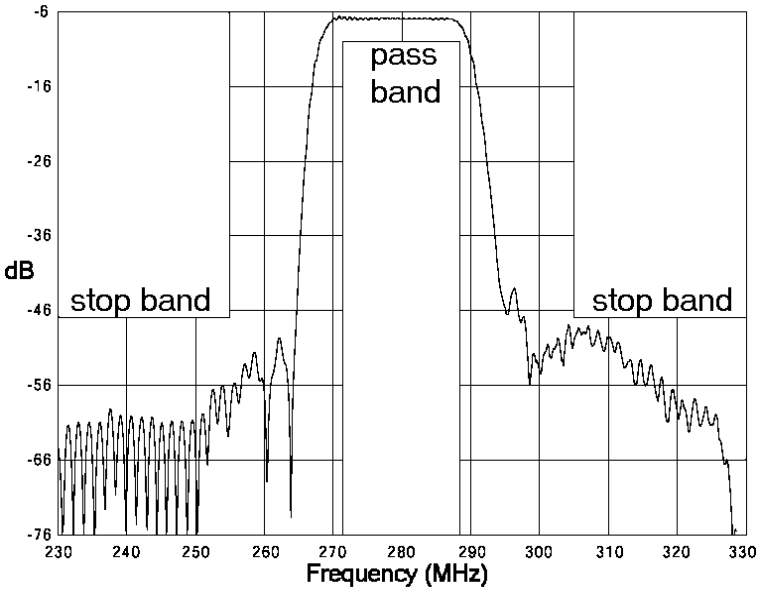

Figure 12: Frequency response of filter for wireless local area network (WLAN). The blocked off areas represent the minimum requirement for the pass band and the stop bands (39).

Table I Most commonly used LN wafer geometries for SAW applications

Crystal	SAW Velocity	Temperature Dependence	Piezo-electric coupling (%)
Y – Z prop	3488 m/s	-94 ppm/ ^{o}C	4.5
128^{o} RY – X prop	3992 m/s	-72 ppm/ ^{o}C	5.3
64° RY – X prop	4742 m/s	-79 ppm/°C	11.3

Shows the three most commonly used LN substrates for SAW devices. The convention is to give the surface normal direction first as an angle rotated away from +Y towards +Z, followed by the propagation direction of the SAW waves. All LN cuts show a temperature sensitivity where the filter characteristics shifts by around 80ppm for every degree in environmental temperature change. This is a problem for narrow bandpass filters or oscillators, so other materials are typically used for those applications. The substrate with the longest use history is the YZ, but it has since been replaced in many applications by 128°RY substrates because of lower bulk-wave excitation. The 64°RY cut is used with leaky surface-waves instead of pure surface waves. Attenuation of such a leaky wave is 7.6dB/mm for a free surface, but negligible for metallized surfaces (40).

Electro-optic Applications of LN.

The electro-optic effect describes how the index of refraction is changed with the application of an electric field. In a common bulk optics application, a Pockels cell rotates the polarization of the light when a voltage is applied. This devices is used for example in Q-switching Nd:YAG lasers. A schematic of such a laser cavity is shown in Figure 13. With no applied voltage, the LN cell does not affect the polarization state of the light because the light propagates along the optical axis. The laser will operate continuously with output polarization aligned with the polarizer as shown. When the voltage is applied, slight changes in refractive index are induced for light polarized along and perpendicular to the electric field. For the correct voltage, the relative phase-retardation of the two polarization components for a double-pass through the cell is 180°. In that case, light exiting the polarizer and propagating to the right will return at a

polarization state that is 90° rotated and thus completely rejected by the polarizer, making laser oscillation impossible. In a typical application, this voltage is applied while the flash lamps pump the laser medium. At the time of maximum gain in the laser rod, the electrodes are shorted, dropping the voltage to zero and enabling the laser radiation to build up so that all the stored energy is extracted from the laser rod into the short pulse.

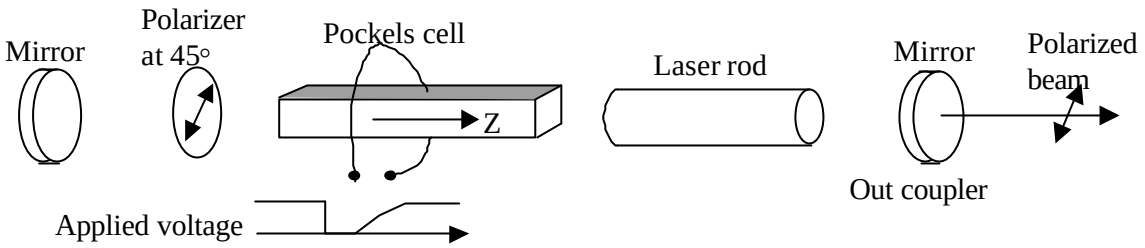

Figure 13: Schematic of laser cavity using LN as Q-switch.

With the increased demand for bandwidth on fiber optic communication lines, LN has gained importance in various integrated optic components(41, 42). Among those, the high speed electro-optic modulator, either fabricated on an X- or a Z-wafer is the most prevalent. The advent of erbium fiber amplifiers has increased the distance between electrical-optical converters and has also enabled wavelength division multiplexing (WDM) where dozens of digital signal streams are launched into the same fiber by using slightly different wavelengths for each of them. LN modulators are well matched to the requirements for WDM systems because they enable fast (40GHz or more) modulation speed at reasonable voltage levels with very low pulse chirp(43).

Figure 14 shows the basic layout of such an intensity modulator. Light is coupled from an incoming fiber (from a continuously emitting laser at a particular wavelength) into the waveguide. At the Y-junction, the energy is split evenly into two waveguide paths. At the second Y-junction, the energy is recombined into the output waveguide and to the fiber. With no voltage applied, the two waves experience the same optical path length in the two arms of the interferometer, and the recombination is perfect so that all the light (except for propagation or coupling losses) is coupled into the receiving fiber. If a voltage is applied to the electrodes, the electrical field inside the crystal at the waveguide location causes an index change, and the path-length for that arm is changed, changing the relative phase of the two optical waves at the second Y-junction. If the voltage applied is V_π, the induced phase change is π, and the two fields from the waveguides are out of phase so that the energy gets radiated into the substrate, and no light is coupled into the waveguide or the fiber.

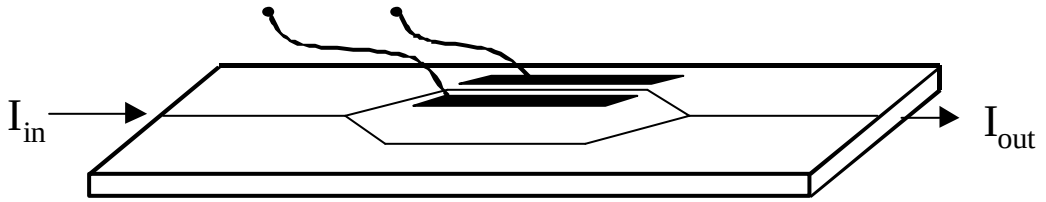

Figure 14: Simplified schematic of integrated optic modulator based on a Mach-Zehnder interferometer.

Optical waveguides are produced in the substrate by a lithography step defining the waveguide channels, followed by a diffusion process. In a titanium in-diffused waveguide, strips of the metal are put down lithographically, involving a lift-off or etching step. The wafer is then heated in a furnace to a temperature around 1000°C to diffuse the metal into the substrate. The

resulting Ti concentration profile gives rise to an increased index, supporting an optical mode.(44) An alternative method to fabricate a waveguide relies on proton-exchange. First, a metal or SiO_2 mask is defined lithographically, leaving the area for the waveguides exposed. The wafer is then dipped into an acid, typically benzoic acid at the melting point, followed by an annealing step at temperatures around 400°C (45). High-speed operation of the modulators requires velocity matching of the electric RF wave with the propagating optical wave. The dielectric constant in LN is large (~30), so the electrodes need to be electroplated to have a significant amount of energy traveling in air, speeding up the traveling microwave. Actual designs can be quite complex, requiring various processing steps such as buffer layer deposition or reactive LN etching (46).

Figure 15 shows the electrode design for a 10GHz modulator on an X-cut LN substrate.(47) Both arms of the interferometer are simultaneously driven. The voltage applied at the hot electrode sets up electric fields overlapping with the optical energy in the waveguides. The index of refraction modulation has opposite sign for the two arms because the field intersects the waveguides in opposite directions with respect to the Z-axis.

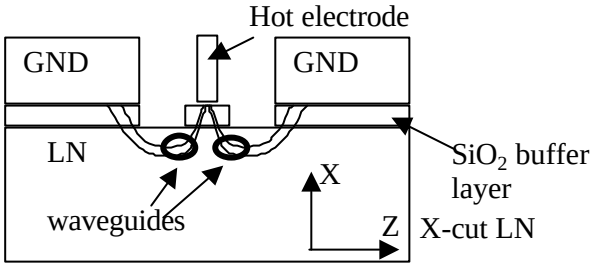

Figure 15: Cross section through traveling wave electrode (after (47)).

Other types of integrated optic devices can also be manufactured on LN. For wavelength-selective demultiplexing of WDM signals, acousto-optic tunable filters can be used.(48) In such devices, a SAW wave is excited to travel between two straight, neighboring optical waveguides. The signal containing all different wavelengths is launched into one of the waveguides. If the frequency of the RF signal generates a SAW with the correct period for a particular wavelength, light of that wavelength is coupled over to the neighboring waveguide and can be detected without affecting the remaining signals.

Other Niobate Crystals

Most niobate crystals other than LN are perovskites and are difficult to grow because they undergo several structural phase-transitions.

Probably the most widely used crystal after LN is potassium niobate ($KnbO_3$, KN) that can be grown from K_2O flux.(49, 50) Poling is performed close to the phase transition temperature at 225°C (Figure 3). Besides having been characterized for its photorefractive and SAW properties, KN mostly has been used to frequency-double diode lasers to the blue range of the visible spectrum. In a fully oxidized state, KN is resistant to photorefractive damage and possesses large nonlinear optical coefficients. The crystal must be treated carefully since any handling or thermally induced stress can lead to generation of 90° domains.

$Ba_2NaNb_5O_{15}$ and the two mixed crystals $K_3Li_{2-x}Nb_{5+x}O_{15+2x}$ (KLN, $0.15<x<0.5$) and $Sr_xBa_{1-x}Nb_2O_6$ (SBN, $x\sim0.6$) show very large permittivities and nonlinear polarizabilities. The first

two have often been investigated for frequency doubling applications to the blue. KLN offers the potential to vary the Li to Nb composition to adjust the Curie temperature and the birefringence in order to match a particular application. However, no congruently melting composition exists and it has been difficult to achieve acceptable uniformity even using sophisticated growth technology.(51) SBN can be congruently grown at x~0.6, and has been studied for electro-optic as well as photorefractive storage applications.(52) Because the Curie temperature at 78°C is close to the operating temperature, electro-optic coefficients are very large and the necessary voltage to drive an integrated modulator is lower by a factor of 16 when compared to a device with similar geometry on LN.(53)

A widely studied group of crystals belongs to the class of relaxor ferroelectrics. Such materials are useful for demanding electro-mechanical actuators or ultrasonic transducers. The material typically used for those application is ceramic $Pb(Zr,Ti)O_3$ (PZT). By adjusting the Zr-Ti composition, the Curie temperature can be adjusted close to room temperature, resulting in piezo-electric coefficients up to 700pC/N. However, PZTs can not be grown as single crystals. Relaxor ferroelectrics on the other hand allow this, most notably the solid solutions of lead magnesium niobate or lead zinc niobate with lead titanate. The addition of lead titanate pushes the compound closer to the tetragonal phase transition, increasing the piezoelectric constant up to 2000pC/N.(54) In $Pb(Zn_{1/3}Nb_{2/3})O_3$ – $PbTiO_3$ (PZN-PT) solid solutions, the PT concentration needs to be at or below 8% to avoid a tetragonal phase, where the concentration for $Pb(Mg_{1/3}Nb_{2/3})O_3$ – $PbTiO_3$ (PMN-PT) can be as high as 35%. The crystals are mostly grown from flux and exhibit extremely high electromechanical coupling (90-94%). The allowable strain is 5 to 6 times higher than in PZT ceramics, allowing much larger energy densities (Figure 16). This enables more compact transducers that deliver more power at increased frequency bandwidth. This is particular important for submarine and medical applications. (e.g. 12dB more power at 1/3 the size for a sonic actuator) New medical imaging systems often involve a transducer radiating at one frequency, and sensing the second harmonic, requiring large bandwidths.

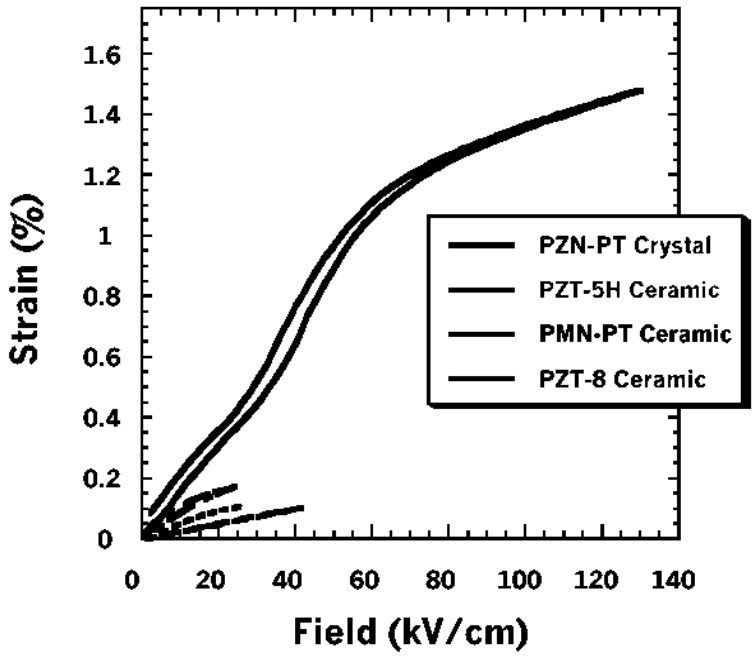

Figure 16: Strain induced in various ceramics and a PZN-PT single crystal. The single crystal has higher sensitivity (slope), and allows many times larger strain values before yielding.(55)

References

(1) A. Räuber, “Chemistry and physics of lithium niobate,” Current topics in materials science, vol. 1, ed. E. Kaldis (Amsterdam: North-Holland, 1978), 481-601.

(2) P. F. Bordui, R. G. Norwood, C. D. Bird, and G. D. Calvert, "Compositional uniformity in growth and poling of large-diameter lithium niobate crystals,” J. Crystal Growth, 113 (1991), 61-68.

(3) Ferroelectrics and related substances, subvolume a: Oxides,” Landolt-Börnstein, Zahlenwerte und Funktionen aus Naturwissenschaften und Technik, Neue Serie, vol. 16, ed. K.-H. Hellwege and A. M. Hellwege (Berlin: Springer-Verlag, 1981).

(4) J. F. Nye, Physical Properties of Crystals, (Oxford: Oxford, 1985).

(5) M. Thirumavalavan, S. Sitharaman, S. Ravi, L. Durai, N. L. Jagota, R. C. Narula, and R. Thyagarajan, "Growth of large diameter lithium niobate single crystals by Czochralski method,” Ferroelectrics (UK), 102 (1990), 15-22.

(6) K. Nassau, H. J. Levinstein, and G. M. Loiacono, "Ferroelectric lithium niobate. 1. Growth, domain structure, dislocations and etching,” J. Phys. Chem. Solids, 27 (1966), 983-988.

(7) D. Cochet-Muchy, "Growth of piezoelectric crystals by Czochralski method,” Journal de physique IV (Colloque), 4 (C2) (1994), 33-45.

(8) T. Tsukada, K. Kakinoki, M. Hozawa, N. Imaishi, K. Shimamura, and T. Fukuda, "Numerical and experimental studies on crack formation in $LiNbO_3$ single crystal,” Journal of Crystal Growth, 180 (1997), 543-550.

(9) N. Miyazaki, H. Uchida, T. Tsukada, and T. Fukuda, "Quantitative assessment for cracking in oxide bulk single crystals during Czochralski growth:development of a computer program for thermal stress analysis,” Journal of Crystal Growth, 162 (1996), 83-8.

(10) R. L. Byer, J. F. Young, and R. S. Feigelson, "Growth of high-quality $LiNbO_3$ crystal from the congruent melt,” J. Appl. Phys., 41 (1970), 2320-2325.

(11) J. G. Bergman, A. Ashkin, A. A. Ballman, J. M. Dziedzic, H. J. Levinstein, and R. G. Smith, "Curie temperature, birefringence, and phase-matching temperature variations in $LiNbO_3$ as a function of melt stoichiometry,” Appl. Phys. Lett., 12 (1968), 92-94.

(12) A. Mendez, A. Garcia-Cabanes, E. Dieguez, and J. M. Cabrera, "Wavelength dependece of electro-optic coefficients in congruent and quasi-stoichiometric $LiNbO_3$,” Electron. Lett., 35 (1999), 498-499.

(13) P. F. Bordui, R. G. Norwood, D. H. Jundt, and M. M. Fejer, "Preparation and characterization of off-congruent lithium niobate crystals,” J. Appl. Phys., 71 (1992), 875-879.

(14) J. Li, I. Kao, and V. Prasad, "Modeling stresses of contacts in wire saw slicing of polycristalline and crystalline ingots: Application to silicon wafer production,” J. Electronic Packaging, 120 (1998), 123-128.

(15) G. J. Edwards and M. Lawrence, "A temperature-dependent dispersion equation for congruently grown lithium niobate," Opt. Quantum Electron., 16, (1984), 373-375.

(16) A. V. Oppenheim and R. W. Schafer, Digital signal processing, (Englewood Cliffs, NJ: Prentice-Hall, Inc., 1975).

(17) H. Fay, W. J. Alford, and H. M. Dess, "Dependence of second-harmonic phase-matching temperature in $LiNbO_3$ crystals on melt composition," Appl. Phys. Lett., 12 (1968), 89-92.

(18) R. L. Byer, Y. K. Park, R. S. Feigelson, and W. L. Kway, "Efficient second-harmonic generation of Nd:YAG laser radiation using warm phasematching $LiNbO_3$," Appl. Phys. Lett., 39 (1981), 17-19.

(19) J. L. Nightingale, W. J. Silva, G. E. Reade, A. Rybicki, W. J. Kozlovsky, and R. L. Byer, "Fifty percent conversion efficiency second harmonic generation in magnesium oxide doped lithium niobate," Proc. SPIE, 681 (1986), 20-24.

(20) R. Paschotta, K. Fiedler, P. Kürz, R. Henking, S. Schiller, and J. Mlynek, "82% efficient continuous-wave frequency doubling of 1.06 μm with a monolithic $MgO:LiNbO_3$ resonator," Opt. Lett., 19 (1994), 1325-1327, errata, 20 (1995), 345.

(21) A. Ashkin, G. D. Boyd, J. M. Dziedzic, R. G. Smith, A. A. Ballman, J. J. Levinstein, and K. Nassau, "Optically-induced refractive index inhomogeneities in $LiNbO_3$ and $LiTaO_3$," Appl. Phys. Lett., 9 (1966), 72-74.

(22) T. R. Volk, N. M. Rubinina, and A. I. Kholodnykh, "Effiecient laser frequency converters made from nonphotorefractive lithium niobate," Sov. J. QuantumElectron., 18 (1988), 1061-1062.

(23) L. E. Myers and W. R. Bosenberg, "Periodically poled lithium niobate and quasi-phase-matched optical parametric oscillators," J. Quantum Electron., 33 (1997), 1663-1672.

(24) M. M. Fejer, G. A. Magel, D. H. Jundt, and R. L. Byer, "Quasi-phase-matched second harmonic generation: tuning and tolerances," IEEE J. Quantum Electron., 28 (1992), 2631-2654.

(25) P. E. Powers, T. J. Kulp, and S. E. Bisson, "Continuous tuning of a continuous-wave periodically poled lithium niobate optical parametric oscillator by use of a fan-out grating design," Opt. Lett., 23 (1998), 159-161.

(26) T. Töpfer, K. P. Petrov, Y. Mine, D. Jundt, R. F. Curl, and F. K. Tittel, "Room-temperature mid-infrared laser sensor for trace gas detection," Appl. Optics, 36 (1997), 8042-8049.

(27) A. M. Glass, D. Von der Linde, and T. J. Negran, "High voltage bulk photovoltaic effect and the photorefractive process in $LiNbO_3$," Appl. Phys. Lett., 25 (1974), 233.

(28) A. Yariv, S. Orlov, G. Rakuljk, and V. Leyva, "Holographic fixing, readout, and storage dynamics in photorefractive materials," Opt. Lett., 20 (1995), 1334-1336.

(29) I. Nee, K. Buse, F. Havermeyer, R. A. Rupp, M. Fally, and R. P. May, "Neutron diffraction from thermally fixed gratings in photorefractive lithium niobate crystals," Phys. Rev. B, 60 (1999), R9896-R9899.

(30) J. J. Amodei and D. L. Staebler, "Holographic pattern fixing in electro-optic crystals," Appl. Phys. Lett., 18 (1971), 540.

(31) S. Breer and K. Buse, "Wavelength demultiplexing with volume phase holograms in photorefractive lithium niobate," Appl. Phys. B, 66 (1998), 339-345.

(32) J. Young, E. H. and S.-K. Yao, "Design considerations for acousto-optic devices," Proceedings of the IEEE, 69 (1981), 54-64.

(33) P. A. Pinnow, "Guide lines for the selection of acoustooptic materials," IEEE J. Quantum Electron., QE-6 (1970), 223-238.

(34) C. C. W. Ruppel, R. Dill, A. Fischerauer, G. Fischerauer, W. Gawlik, J. Machui, F. Muller, L. Reindl, W. Ruile, G. Scholl, I. Schropp, and K. C. Wagner, "SAW devices for consumer communication applications," IEEE Trans. Ultrasonics, Ferroelectrics, and Frequ. Control, 40 (1993), 438-452.

(35) J. Machui, J. Bauregger, G. Riha, and I. Schropp, "SAW devices in cellular and cordless phones," Proceedings of the 1995 Ultrasonics Symposium, (1995), 121-130.

(36) D. P. Morgan, "History of SAW devices" (Paper presented at 1998 IEEE international frequency control symposium, 1998), 439-460.

(37) R. F. Mitchell, "Acoustic surface-wave filters," Philips tech. Rev., 32 (1971), 179-189.

(38) C. K. Campbell, "Applications of surface acoustic and shallow bulk acoustic wave devices," Proceedings of the IEEE, 77 (1989), 1453-1484.

(39) M. Bracewell, Product literature SAWTEK, Inc. (Saw science), 13 (1998), 5.

(40) K. Yamanouchi and M. Takeuchi, "Applications for piezpelectric leaky surface waves," Proceedings of the 1990 Ultrasonics Symposium, (1990), 11-18.

(41) S. S. Bosso, "Applications of lithium niobate integrated optic in telecommunication systems," Proceedings of SPIE, Integrated Optics Devices III, 3620, (1999), 34-37.

(42) D. Fritz, G. McBrien, and P. G. Suchoski, "Practical applications for integrated optics in communications systems," Proceedings of SPIE, Integrated Optics Devices IV, 3936, (2000), 218-221.

(43) E. L. Wooten, K. M. Kissa, A. Yi-Yan, E. J. Murphy, D. A. Lafaw, P. F. Hallemeier, D. Maack, D. V. Attanasio, D. J. Fritz, G. J. McBrien, and D. E. Bossi, "A review of lithium niobate modulators for fiber-optic communications systems," IEEE Journal of Selected Topics in Quantum Electronics, 6 (2000), 69-82.

(44) S. Fouchet, A. Carenco, C. Daguet, R. Guglielmi, and L. Riviere, "Wavelength dispersion of Ti induced refractive index change in $LiNbO_3$ as a function of diffusion parameters," J. Lightwave Techn., LT-5, (1987), 700-708.

(45) D. K. Lewis, K. M. Kissa, and P. G. Suchoski, "Long lifetime projections for annealed proton-exchanged waveguide devices," IEEE Photonics Techn. Lett., 7 (1995), 200-202.

(46) K. Noguchi, O. Mitomi, K. Kawano, and M. Yanagibashi, "Highly efficient 40-GHZ Bandwidth Ti:$LiNbO_3$ optical modulator employing ridge structure," IEEE Photonics Technology Lett., 5 (1993), 52-54.

(47) Y. Miyama, T. Sugamata, Y. Hashimoto, T. Sakamoto, and H. Nagata, "Novel X-cut lithium niobate intensity modulator with 10G bandwidth," Proceedings of SPIE, Conference on Optical Devices for Fiber Communication, 3847, (1999), 102-109.

(48) D. A. Smith and J. J. Johnson, "Surface-acoustic-wave directional coupler for apodization of integrated acousto-optic filters," IEEE Trans. on Ultrasonics, Ferroelectrics and Frequency control, 40 (1993), 22-25.

(49) W. Xiang, H. Looser, H. Wuest, and H. Arend, "Progress in $KNbO_3$ crystal growth," J. Cryst. Growth, 78 (1986), 431-437.

(50) G. Mizell, W. R. Fay, and T. Alekel III, "Growth, properties, and applications of potassium niobate single crystals," SPIE, Visible and UV lasers, 2115, (1994), 19-30.

(51) M. Ferriol, G. Foulon, A. Brenier, M. T. Cohen-Adad, and G. Boulon, "Laser heated pedestal growth of pure and Nd^{3+}-doped potassium lithium niobate single-crystal fibers," J. Cryst. Growth, 173 (1997), 226-230.

(52) R. R. W. F. Hall, J. R. Oliver, and W. K. Cory, "Tungsten bronze $Sr_{1-x}Ba_xNbO_6$: A case history of versatility," Ferroelectrics, 87 (1988), 167-179.

(53) O. Kwon, O. Eknoyan, H. F. Taylor, and R. R. Neurogaonkar, "Low-voltage electro-optic modulator in SBN:60," Electron. Lett., 35 (1999), 219-220.

(54) S. E. Park and T. R. Shrout, "Relaxor-based ferroelectric single crystals for electromechanical actuators," Materials Reserach Innovations, 1, (1997), 20-25.

(55) "Single Crystals" data sheet, (TRS Ceramics, Inc., 2000).